Seasonal trends of nighttime plasma density enhancements in the topside ionosphere

Ewa Slominska, Jan Blecki, Jean-Pierre Lebreton, Michel Parrot, Jan Slominski

AGU PUBLICATIONS

JGR

Journal of Geophysical Research: Space Physics

RESEARCH ARTICLE

10.1002/2014JA020181

Key Points:
- Ionospheric anomalies resembling the Weddell Sea Anomaly (WSA)
- Spatial and temporal characteristics of the WSA-like phenomena
- Electron density during deep solar minimum

Supporting Information:
- Text S1
- Animation S1

Correspondence to:
E. Slominska,
ewaslominska@icloud.com

Citation:
Slominska, E., J. Blecki, J.-P. Lebreton, M. Parrot, and J. Slominski (2014), Seasonal trends of nighttime plasma density enhancements in the topside ionosphere, *J. Geophys. Res. Space Physics*, *119*, 6902–6912, doi:10.1002/2014JA020181.

Received 15 MAY 2014
Accepted 31 JUL 2014
Accepted article online 11 AUG 2014
Published online 27 AUG 2014

Seasonal trends of nighttime plasma density enhancements in the topside ionosphere

Ewa Slominska[1], Jan Blecki[2], Jean-Pierre Lebreton[3], Michel Parrot[3], and Jan Slominski[2]

[1]OBSEE, Warsaw, Poland, [2]Space Research Center PAS, Warsaw, Poland, [3]LPC2E, Orleans, France

Abstract In situ registrations of electron density from the Langmuir probe on board Detection of Electro-Magnetic Emissions Transmitted from Earthquake Regions satellite are used to study spatial and temporal evolution of nighttime plasma density enhancements (NPDEs). The study introduces the normalized density difference index I_{NDD} in order to provide global estimates of the phenomenon. In the validation test, in situ data are compared with synthetic data set generated with the International Reference Ionosphere model. We find signatures of two most common examples of NPDEs, the Weddell Sea Anomaly (WSA) and midlatitude nighttime summer anomaly (MSNA) with proposed index, in the topside ionosphere. The study provides evidence that the occurrence of the WSA and MSNA is not limited to the local summer conditions. Analyzed annual trend of I_{NDD} and in particular spatial pattern obtained during equinoxes suggest that mechanisms governing the behavior of the equatorial ionosphere cannot be neglected in the explanation of the development of NPDEs.

1. Introduction

The problem of the Weddell Sea Anomaly (WSA) has focused attention of many researchers from the early stage of its discovery during the International Geophysical Year (1957–1958) [*Penndorf*, 1965, and references therein]. Ionospheric F_2 layer, above the Antarctic Peninsula and surrounding seas: the Weddell Sea and the Bellingshausen Sea, revealed a distinctive diurnal cycle, which was characterized by greater electron density measured at night than during the day in summer. The phenomenon, initially diagnosed with data obtained from the network of ionosondes spread across Antarctica and the Falkland Islands, has widely attracted scientific communities when new observational techniques became available. In particular, the increasing number of satellite observations opened new possibilities for better exploration of the WSA phenomenon.

Extensive studies based on analysis of total electron content from the altimeter on TOPEX/Poseidon provided by *Horvath and Essex* [2003] and *Horvath* [2006] pointed out that the spatial area of the WSA is greater than it was initially assumed. Further analysis involving not only altimeter missions TOPEX/Poseidon and Jason-1 [*Jee et al.*, 2009] but also measurements from the FORMOSAT-3/COSMIC Constellation [*Burns et al.*, 2008, 2011; *Lin et al.*, 2010], Thermosphere, Ionosphere, Mesosphere Energetics and Dynamics/Global Ultraviolet Imager [*Hsu et al.*, 2011], and DMSP [*Horvath and Lovell*, 2010] brought the confirmation. Furthermore, the same data sources provided evidence of similar feature in the Northern Hemisphere, which was named the midlatitude summer nighttime anomaly (MSNA) [*Thampi et al.*, 2009; *Lin et al.*, 2010; *Thampi et al.*, 2011] or summer evening anomalies (SEAs) [*Burns et al.*, 2011]. The most prominent manifestation of the MSNA was observed in the Northeast Asia, Europe/Africa, and Central Atlantic longitudes around June solstice. *Hsu et al.* [2011] and *Ren et al.* [2012] extended analysis of MSNA over equinoxes and confirmed that MSNA not only occurs in local summer but also often occurs in equinox. Recently, *Zhang et al.* [2013] investigated the so-called midlatitude arcs (MLA) as an example of the nightside enhancements of ionospheric electron density at 20°–45° magnetic latitudes in both hemispheres, and concluded that MLAs are not only typical during local summer. In the present analysis, we use more general name for both types of anomalies, calling them nighttime plasma density enhancements (NPDEs). This is because we note that this phenomenon is not only limited to local summer conditions. Furthermore, we find out that NPDEs span over large regions, therefore using the term anomaly may be inaccurate.

In order to achieve better understanding and give fuller image of processes linked with observed WSA or WSA-like phenomena, *Horvath and Lovell* [2009a, 2009b] and *Horvath and Lovell* [2010] provide comprehensive studies utilizing multiinstrumental data from the DMSP satellites. The analysis examines ion

density, electron and ion temperature, vertical and horizontal plasma drifts, and fractional amounts of ions O^+ and H^+, followed by derived values of vertical and horizontal plasma fluxes. Though numerous studies distinguish major pieces of this puzzle, full explanation of mechanisms governing development of WSA and MSNA seems to be still missing. Up to date reviews can be found in papers by *Burns et al.* [2011], *Chen et al.* [2011], and *Zhang et al.* [2013, and references therein], but we list most common aspects below.

Configuration of the Earth's magnetic field organizes the spatial distribution of WSA [*Horvath and Essex*, 2003] and also NPDEs. Neutral winds in the lower layers of the ionosphere are considered a fundamental phenomenon responsible for accumulation of ionospheric plasma and its maintenance at higher altitudes [*Rishbeth*, 1998; *Jee et al.*, 2005; *Horvath*, 2006]. *Chen et al.* [2011] performed simulations with the ionospheric model SAMI2 in order to estimate importance of $\mathbf{E} \times \mathbf{B}$ drift and neutral winds as leading ways of the plasma transport. The role of equatorward neutral wind is greater, and it should serve as the critical driver for the WSA formation. On the other hand, there are numerous doubts about the efficiency of this mechanism. *Burns et al.* [2008] discussed how temperature and neutral composition changes were not the probable cause of the WSA but suggested that an evening downward flux of plasma from the plasmasphere has the potential to satisfy the observational constraints and may be at least partly responsible for the phenomenon. *Tsagouri and Belehaki* [2002] came to a similar conclusion in the study oriented on a potential sources of nighttime ionization enhancements and nighttime F_2 uplifting. *Tsagouri and Belehaki* [2002] found that wave-like disturbances that most probably originate in the auroral oval region and propagate toward the equator like traveling ionospheric disturbances are typical for an uplifting in the F_2 layer. However, in terms of f_0F_2 observations, ionization enhancements do not share the same wave-like character. Therefore, authors emphasized the important role of downward fluxes from the plasmasphere, which can modify the value of h_mF_2 and contribute to the increased height observation.

Additionally, *Burns et al.* [2008] and *Horvath and Lovell* [2009a] inquired into the idea that there is a connection between equatorial ionization anomaly and observed WSA and MSNA. Finally, in the attempts toward explanation of SEAs, *Burns et al.* [2011] examined conjugated electric fields and suggested that the critical factor in producing the density enhancements and the WSA appears to be that they only occur when a flux tube is illuminated in one hemisphere and in darkness in the other end, what leads to asymmetric conductivity between summer and winter hemispheres. According to *Burns et al.* [2011], one end of the flux tube is in the highly conductive *E* region, where the neutral winds cause a strong dynamo effect, while the other end is in the poorly conducting F_2 with weak horizontal currents. Not sufficient velocities of ion drifts, needed to transport ions from the equatorial boundary, are considered as one of the major drawbacks of the proposed approach. Thus, surge of ions by $\mathbf{E} \times \mathbf{B}$ drift followed by downward movement along the field lines as a result of ambipolar diffusion is acknowledged as a contributing factor.

Among all mentioned phenomena, the components of the Earth's magnetic field are unquestionable factors controlling the spatial distribution of observed NPDEs. With the results presented in the forthcoming sections, we aim to analyze the response of the topside ionosphere to WSA-like phenomena, as well as verify which processes play fundamental role in the observed pattern. The paper is organized in the following way. Section 2 outlines approach based on the definition of the I_{NDD} index and gives an overview of the data set. Results are presented in section 3 and discussed in section 4. Section 5 summarizes and concludes major findings.

2. Method and Data Set

2.1. Estimates of Plasma Density Difference

The present analysis makes use of in situ electron density N_e measurements gathered by the Instrument Sonde de Langmuir (ISL) probe mounted on board Detection of Electro-Magnetic Emissions Transmitted from Earthquake Regions (DEMETER) satellite and also utilize numerical simulations from the commonly used ionospheric model, International Reference Ionosphere (IRI)-2012 (http://iri.gsfc.nasa.gov/) [*Bilitza et al.*, 2011]. The main goal of the study is to provide a global map of regions in which nighttime plasma density enhancements occur and then examine temporal changes. In order to achieve stated goals, we introduce the index I_{NDD} which estimates the values of normalized density difference in each cell of a global map grid. The principles of applied method rely on the fact that DEMETER had the Sun-synchronous orbit, providing information on the ionospheric conditions only for 2 h during the whole day: shortly before the noon (10:30 LT) and several hours after sunset (22:30 LT), thus the image that unveils from the data is a kind of snapshot for ionospheric conditions. When the same local time for each location is plotted together,

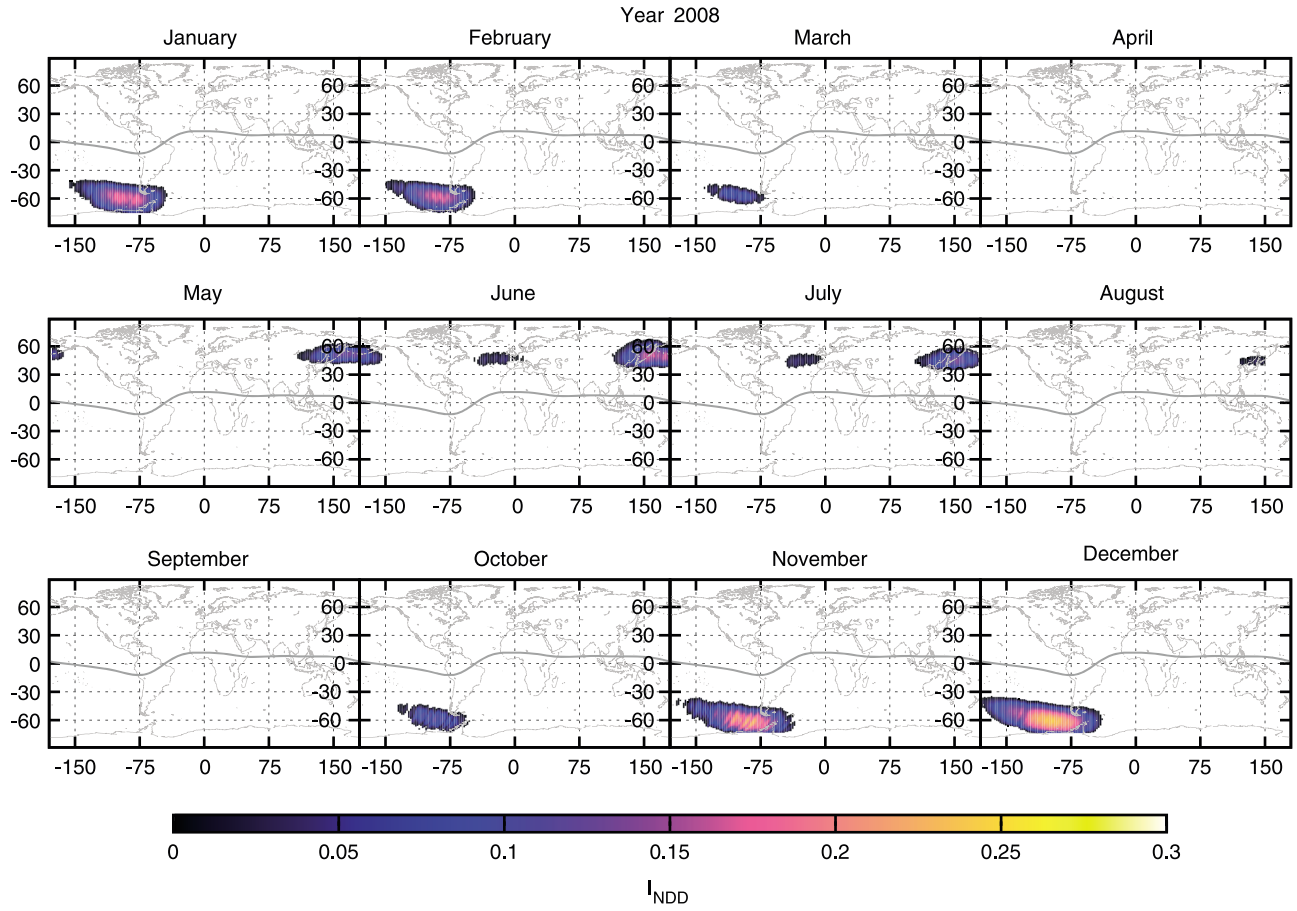

Figure 1. Monthly evolution of I_{NDD} index derived from synthetic data generated with IRI2012 model, year 2008. For the ease of identification of anomalous regions, only $I_{NDD} > 0$ is plotted.

the variations due to geographic location (instead of time) can easily be seen; however, we encounter limitations regarding diurnal variability.

I_{NDD} index is expressed by the formula

$$I_{NDD}(\lambda,\theta) = \frac{N_e^{night}(\lambda,\theta) - N_e^{day}(\lambda,\theta)}{N_e^{night}(\lambda,\theta) + N_e^{day}(\lambda,\theta)}, \quad (1)$$

in which λ denotes geographic longitude, θ geographic latitude, while N_e^{day} and N_e^{night} denote electron density measured on daytime and nighttime DEMETER overpasses, respectively. Evaluation of differences between nighttime and daytime N_e in the context of identification of the WSA-like phenomena was already presented by *Lin et al.* [2010] and *deLarquier et al.* [2011]; however, in cited studies absolute difference was considered. Since I_{NDD} is additionally normalized, therefore obtains values within the limits from −1 to 1, making it easily adaptable parameter for comparison with other data sources. Under regular condition, negative values represent typical ionospheric behavior following diurnal cycle, while positive values should indicate possible nighttime enhancements. Proposed analysis fits into climatological approach what implies that we analyze relatively long time periods (from weeks to months). For the development of global maps, we use geographic coordinates and mercator projection, while data are binned into grid with the resolution of 2° × 0.5° (longitude × latitude). Spatial resolution depends on the considered time period but for the examined amount of data utilized resolution provides satisfactory results.

2.2. DEMETER Data

Presented study exploits data covering time period, which belongs to very low and unusual solar activity. In the analysis we utilized the years 2005 to 2010 of in situ measurements of electron density N_e acquired by the Langmuir probe mounted on board the DEMETER satellite. On 29 June 2004 French microsatellite

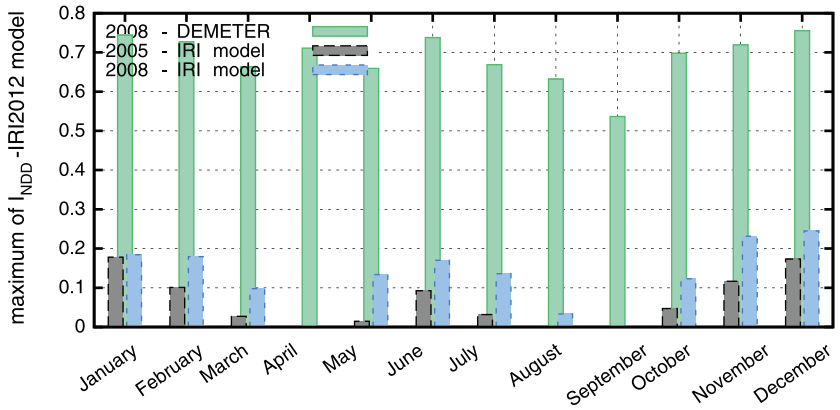

Figure 2. Comparison of maxima of I_{NDD} derived from IRI2012 for years 2005 (gray boxes) and 2008 (blue boxes) and in situ DEMETER data.

named DEMETER (Detection of Electro-Magnetic Emissions Transmitted from Earthquake Regions), operated by Centre National d'Etudes Spatiales, was launched on a Sun-synchronous quasi-circular orbit with an inclination of about 98° and initial altitude of about 710 km, later on reduced to 620 km. The satellite was passing over equator shortly before the local noon at 10:30 in the descending node, and revisiting at 22:30 local time, in the ascending node. The orbital period was around 100 min and spanned the regions between −65° and +65° of invariant latitude. Due to technical constraints, the instruments on board DEMETER were being switched off at higher latitudes in order to minimize the risk of potential failure resulting from higher levels of radiation. The final science commands were received on board DEMETER at the beginning of December 2010 and shortly after the mission was brought to an end. DEMETER was equipped with several instruments, giving an opportunity to perform multiinstrumental in situ registrations in the topside ionosphere. The scientific payload included IMSC (Instrument Magnetometre Search-Coil), three magnetic sensors from a few Hz up to 18 kHz; ICE (Instrument Champ Electrique), three electric sensors from DC (direct current) up to 3.5 MHz; IAP (Instrument Analyseur de Plasma), an ion analyzer oriented on the thermal ion population (density of main components, temperature, and flow velocity); and IDP (Instrument Detecteur de Plasma), an energetic particle detector operating in three energy channels. Presented analysis concentrates on the measurements from the ISL (Instrument Sonde de Langmuir) instrument, a Langmuir probe providing electron concentration N_e and temperature T_e with 1 s time resolution. N_e could be measured in the range of 10^8–$5 \cdot 10^{11}$ e/m^3 and T_e in the range of 600–10,000 K, with accuracies of ±30% for N_e and ±15% for T_e. *Lebreton et al.* [2006] in details described theoretical assumptions for the instrument, as well as discussed initial results obtained during the first year of the DEMETER mission. *Kakinami et al.* [2011] discussed spatial and temporal analysis of N_e and T_e from the ISL probe, providing global maps of these two quantities. Moreover, extended studies oriented on the validation of ISL DEMETER N_e and T_e readings with synthetic data set generated with the IRI2012 model were presented by *Slominska and Rothkaehl* [2013].

3. Results

3.1. Synthetic Observation Data—I_{NDD} From IRI2012 Model

Reliability of the I_{NDD} index was tested on data set simulated with the IRI2012 model. To asses possibly similar conditions for validation, the model was set up in such a way as to allow "point-to-point" reconstruction of the whole DEMETER mission with respect to orbit's parameters (time, longitude, latitude, altitude) as well as solar activity. Spatial and temporal evolution is illustrated on monthly maps gathered in Figure 1. In order to easily distinguish anomalous regions, only positive values of the I_{NDD} index have been mapped.

Simulations show that WSA starts to develop in October reaching maximum in December ($\max(I_{NDD}) = 0.24$). From January till March, it substantially vanishes. In the Northern Hemisphere, we identify signatures of the MSNA between May and August with the greatest spatial extent and the largest amplitude of I_{NDD} found in June ($\max(I_{NDD}) = 0.17$). Nighttime density enhancements in the Northern Hemisphere occur in two separate regions, one over Atlantic and the second one over Eastern Coasts of Asia from Kamchatka through the Okhotsk Sea and the Berring Sea reaching Alaska. Varying solar activities impact

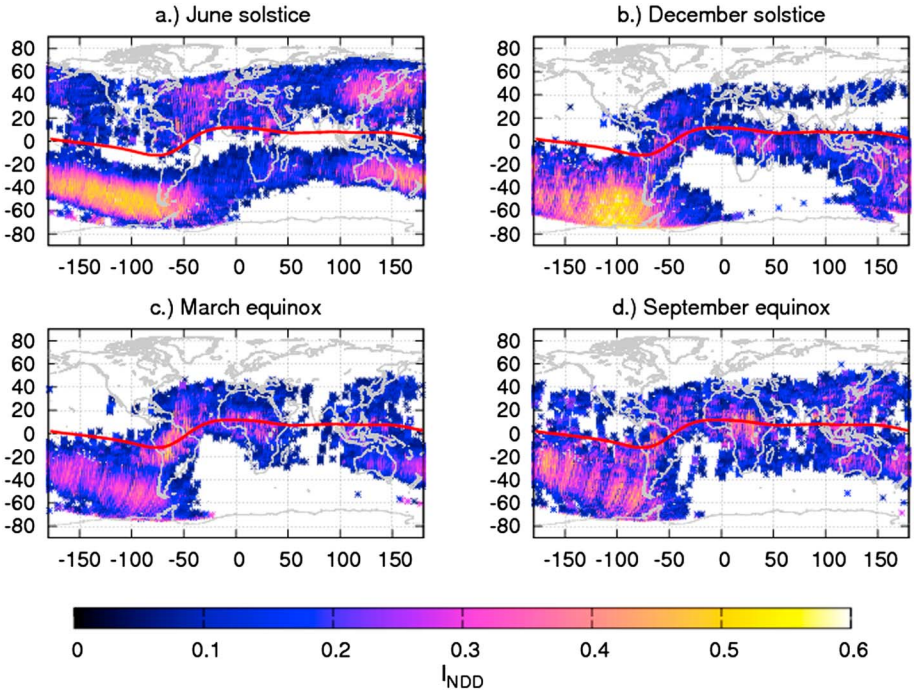

Figure 3. Averaged $I_{NDD} > 0$ plotted for (a, b) solstice and (c, d) equinox conditions.

amplitude of the simulated I_{NDD}, which tends to decrease with increasing solar activity (see Figure 2 for confirmation—comparison between years 2005 ($F_{10.7}$ medium) and 2008 ($F_{10.7}$ low)).

3.2. I_{NDD} Based on the DEMETER ISL N_e Data

$I_{NDD} > 0$ derived from in situ data spreads over much larger regions with 2 times greater amplitude when compared with IRI2012 simulation. Evident amplitude discrepancy of I_{NDD} may originate from instrumental precision, as well as from not ideal representation of the topside ionosphere in the IRI model [*Slominska and Rothkaehl*, 2013, and references therein]. Resemblance between model and data is evident, though on the contrary to the IRI model, NPDEs in the Southern Hemisphere prevail in all seasons.

Figure 3 exhibits four separate maps of spatial distribution of I_{NDD} for distinct ionospheric conditions: both solstices (Figure 3a—June and Figure 3b—December) and both equinoxes (Figure 3c—March and Figure 3d—September). Presented maps are composed from weekly sets of DEMETER overpasses centered on a day of equinox or solstice over six consecutive years of the DEMETER mission (2005–2010). Averaged maps are accompanied by 1 year cycle of monthly maps of I_{NDD} picked for the year 2008 (see Figure 4) characterized by solar ionizing radiation at the lowest levels ever recorded. Annual evolution incorporated to the studies helps to comprehend obtained spatial morphology of I_{NDD}.

Figures 3 and 4 show that plasma density enhancement in the region of the Antarctic Peninsula, the Weddell Sea, and the Belingshausen Sea, as well as in the Southern Pacific Ocean, is observed constantly in the entire analyzed data set; however, the magnitude and the spatial structure vary with time. The WSA itself exhibits both longitudinal and latitudinal variations. Its development over a wider area of the Southern Pacific Ocean is due to the significant photoionization taking place throughout the summer nights as the ionosphere remains illuminated between November and February (local summer—Figure 3b, Figure 4—months: November-December-January-February). During southern local summer (panel b. Figure 3, Figure 4—months: December-January-February) NPDE is widely spread over the whole area of the southern waters of Pacific, nearly approaching the magnetic equator.

In the longitudinal extent, the South Atlantic Anomaly seems to set up one boundary, while in the westward direction, the anomalous region stretches to the eastern coasts of Australia. During other seasons, when local summer comes to an end, the enhancement from the WSA region tends to taper, loosing its poleward and equatorward extent, but still has a shape of prominently elongated bulge. We see that during southern local winter conditions (June case in Figure 3a and months May-June-July-August in Figure 4), it covers

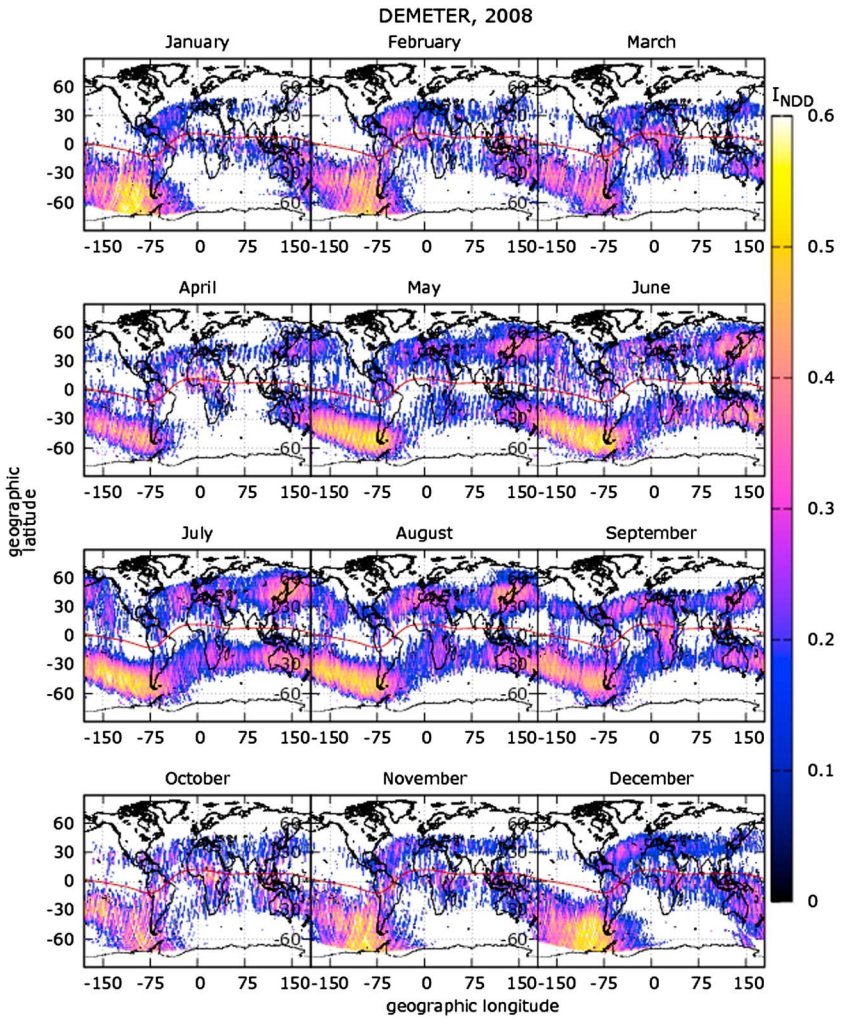

Figure 4. Annual cycle of I_{NDD}. Monthly maps of positive values of I_{NDD} derived from the DEMETER ISL N_e data.

most part of Australia. At the same time, broad areas of amplified I_{NDD} are also present over the Northern Hemisphere, what manifests the signatures of the MSNA.

Compelling image emerges during equinoxes in April and as well as in October. Despite slightly reduced amplitude, I_{NDD} is still accentuated in the midlatitude zones of both hemispheres, but additionally it boosts in the equatorial region in three separate spots: in the Brazilian sector in South America (30°W–75°W), in the central Africa (10°E–50°E), and over Indonesia, Malaysia, and Philippines (100°E–150°E).

In the supporting information we provide animated annual evolution of the $I_{NDD} > 0$ index for every month during six considered years. A closer look at the whole seasonal cycle of $I_{NDD} > 0$ gives the better insight into the dynamic of I_{NDD} parameter and helps to identify discussed basic characteristics.

4. Discussion

Summarizing acquired sessional and spatial distribution of I_{NDD}, we stress out major aspects which dominate in the development process of NDPEs. Foremost factor responsible for the obtained spatial morphology of I_{NDD} is the Earth's magnetic field, which determines longitudinal variability. Gradual expansion and contraction of I_{NDD} in both hemispheres, as well as cyclic movement of maxima of I_{NDD} to both sides of magnetic equator, are consistent with the role of interhemispheric plasma transport [*Heelis and Hanson*, 1980; *Rishbeth*, 1998; *Venkatraman and Heelis*, 1999; *Bailey et al.*, 2000] and indicate the importance of neutral winds, guiding the plasma along the magnetic field lines. Furthermore, NPDEs in the midlatitudes coexist

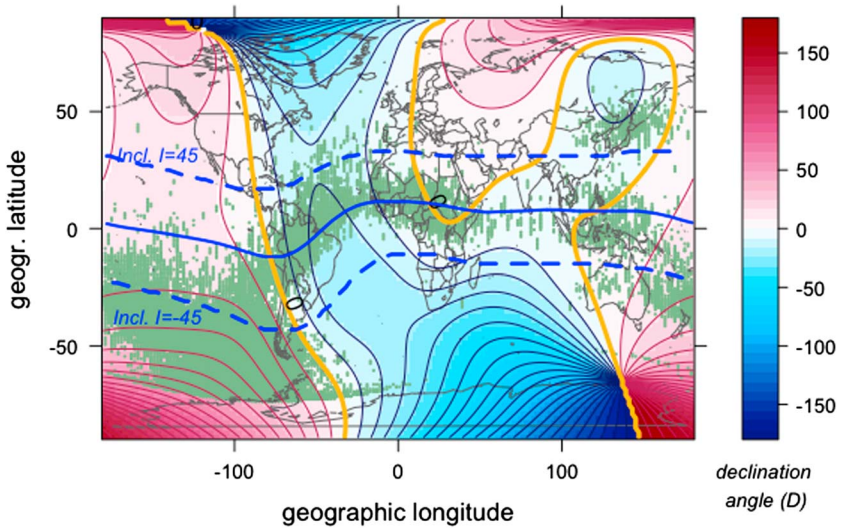

Figure 5. Maxima of I_{NDD} (olive-green points) mapped onto the global map of the Earth's magnetic field declination taken from the International Geomagnetic Reference Field 2010 (IGRF-10) model. Dip angles of $I = \pm 45°$ marked with dashed blue lines indicate location where meridional winds maximize. Yellow solid lines denote $D = 0$ where declination changes from eastward to westward.

with similar enhancements in the equatorial regions; thus, the fountain effect may contribute in the development and maintenance of NPDEs.

Tracking the most intensive vertical upward plasma flows in the nighttime WSA region, *Horvath and Lovell* [2009a] demonstrated the strong importance of the thermospheric neutral winds in its development. While production of the ionosphere is governed primarily by variations of solar radiation, the transport effects caused by electric fields and thermospheric winds depend on magnetic field geometry, with a pattern that has obvious longitude variations. Previous section proves that spatial distribution and occurrence of NPDEs are substantial and repeatable with distinct patterns, exhibiting correspondence with the Earth's magnetic field components. In order to assess confirmation, the utmost values of I_{NDD} have been extracted and mapped onto the global map of magnetic declination (D) taken from the International Geomagnetic Reference Field 2010 (IGRF-10) model (see Figure 5). Magnetic declination, which exhibits longitudinal variability, strongly organizes the effects of neutral winds. Direct relation between neutral winds components and the Earth's magnetic field components was discussed by *Titheridge* [1995], *Rishbeth* [1998], *Jee et al.* [2005], and *Horvath* [2006]. The effective neutral wind which can drag the plasma along the magnetic field is superimposed from drift velocities components of meridional (W_M) and zonal (W_Z) neutral winds and strictly organized by magnetic field inclination (I) and declination (D), as expressed by the formula

$$V_{\text{eff}} = 0.5(W_M \cos D \mp W_Z \sin D) \cdot \sin 2I. \quad (2)$$

The "−" sign applies in the Northern Hemisphere, while "+" in the Southern Hemisphere. In the midlatitude ionospheric F layer, the zonal winds are mainly westward before the dawn and eastward after dusk. The direction of meridional winds is poleward during the day and equatorward at nighttime [*Titheridge*, 1995]. The poleward neutral wind during the day moves the plasma to lower altitudes decreasing the plasma density due to the larger recombination rate. After sunset the upward movement of the plasma by the equatorward wind contributes to maintaining the plasma density at night.

We can roughly gauge the V_{eff} for midlatitudes using formula 2. Assuming equal amplitudes of W_M and W_Z and taking D and I configuration for latitudes of 50°N/S, we would find that in the Southern Hemisphere the contributing net effect of V_{eff} maximizes in the longitude sector of 100°W, while in the Northern Hemisphere amplitude is lower but two separate maxima are distinguished (40°W and 150°E). Using DEMETER data, we find that at midlatitudes in the Southern Hemisphere NPDEs are observed where D is positive, exactly in the regions where plasma is pushed upward. By contrast, in the Northern Hemisphere $D < 0$ supports plasma lifting that coincides with the occurrence of NPDEs in the longitude sector of Eastern Asia. According to *Horvath and Lovell* [2010] the WSA reaches the lowest geographic latitude at around 45°S dip latitude along

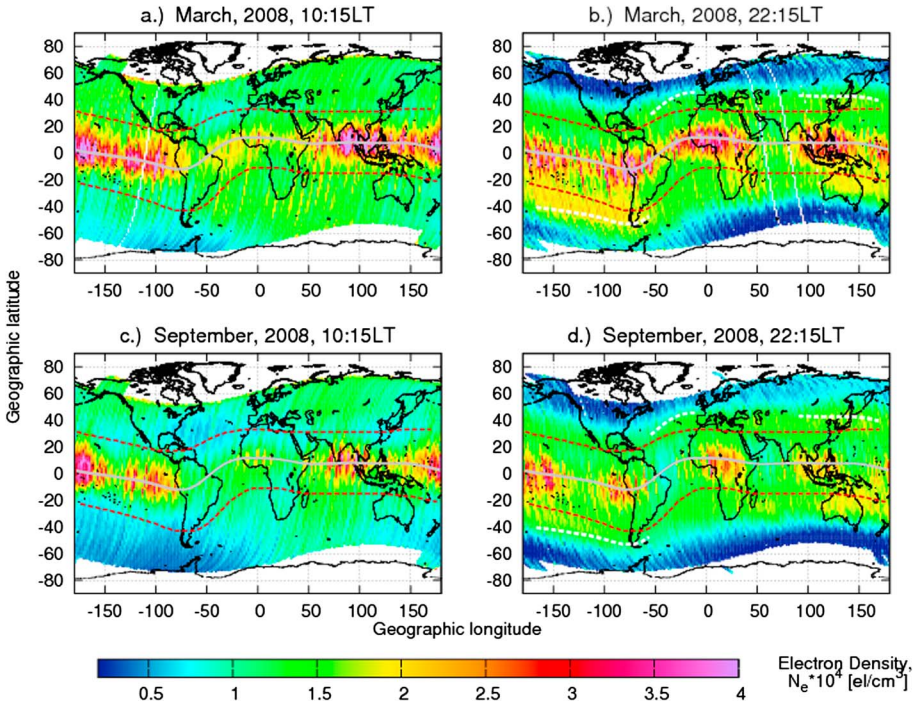

Figure 6. Comparison of monthly plots of the electron density derived for available local times for March and September equinox. Monthly maps of N_e for (left) 10:15 LT and (right) 22:15 LT. Grey solid line indicates the magnetic equator; red dashed lines denote region where magnetic inclination is equal to 45° ($I = 45°$). White dashed lines indicate the edges corresponding to the boundary of the nighttime density anomaly.

the magnetic field line that passes through its center. In Figure 5 the dip angle $I = \pm 45°$ is marked with thick blue dashed lines to indicate the region where V_{eff} maximizes, while little or no impact on height change is expected for $I = 0°$ and $I = 90°$.

In the statistical analysis based on DMSP data, *Horvath and Lovell* [2009a] identified WSA's equatorward boundary as a trough, which develops at (47.1564 ± 2.16)°S, while its poleward limit as the plasmapause. Regarding the nighttime WSA's thermal structures, its equatorward boundary was marked by elevated subauroral ion and electron temperatures, and its poleward boundary was indicated by the highest subauroral electron temperatures. Additionally, neighboring South Atlantic Magnetic Anomaly influences both, WSA and a trough. In corresponding studies oriented on the Northern Hemisphere, *Horvath and Lovell* [2009b] found that northern summer plasma enhancements resembled the nighttime WSA. Their plasma density increased mainly owing to the mechanical or direct effects of the equatorward winds; therefore, the WSA-like feature was considered as an ordinary northern midlatitude nighttime enhancement occurring in summer. The WSA-like related northern trough appeared at significantly higher latitudes, (62.461 ± 2.93)°N (geomagnetic), poleward of the WSA-like feature, and other midlatitude plasma enhancements.

Scrutinizing separately daytime and nighttime maps of N_e (set of maps for equinoxes is gathered in Figure 6) in the nighttime data, we observe enhanced surge of electron density displaced poleward from the marked $I = \pm 45°$ and followed by sharp steep gradients in electron density. Although in the attached comparison, months of equinoxes were selected in order to guarantee relatively uniform solar heating to both hemispheres, we note the surge to be significantly more pronounced in the Southern Hemisphere, along the Pacific Ocean, across Australia and partly in the Indian Ocean. In the Northern Hemisphere its signs are less obvious but still present. The space shift between the poleward edge of the surge and $I = \pm 45°$ is approximately 10°, while maximum of poleward extent is reached at 54°S and 45°N in the Southern and Northern Hemispheres, respectively. Observations from DEMETER coincide with major findings from DMSP data by *Horvath and Lovell* [2009a] and identified WSA's equatorward boundary as a trough.

Dip angles of $I = \pm 45°$ mark a noticeable boundary for NPDEs; however, in the inner, equatorial region separate array of positive I_{NDD} is found. As shown in the previous section and summarized in Figure 5,

NPDEs occurring in the equatorial region additionally reveal nodal structure, with tendency to occupy three separate locations. Such result is considered a manifestation of the **E** × **B** drift and suggests that explanation of NPDEs in the framework of mechanism typical for equatorial ionosphere should be included in the explanation.

The large drift perturbations near sunset can raise the *F* peak to heights above 800 km and produce anomalously large plasma densities at magnetic latitudes beyond 30°. The same uplifts are responsible for postsunset spread-*F* structures and the appearance of intense radio scintillation [*Rishbeth*, 2000]. Despite the not satisfactory modeling results in the studies performed by *Chen et al.* [2011], in situ observations suggest that dynamics of the equatorial region affects also the occurrence of NPDEs. As noticed by *Burns et al.* [2008], enhanced electron densities that appear to be associated with the southern equatorial anomaly are displaced far southward at dusk and, within about an hour, form the WSA. Significant longitudinal variations in the distribution of ionospheric plasma at low latitudes and midlatitudes are controlled by the field-aligned plasma transport and chemical processes. Owing to the spatial variability of ionospheric E field and geomagnetic B field, the equatorial vertical **E** × **B** drift-induced movement also varies, and the following field-aligned plasma flow is modulated by a variable wind transport moving the plasma along the magnetic field lines to altitudes of different recombination rates. Gathered results support the idea. Since observations are carried out in the topside ionosphere, typical for lower layers crests of enhanced electrons density on both sides of the dip equator are not so evident, and instead, asymmetry of ionization bulge may be observed. Such an asymmetry combined with southward displacement of the dip equator results in expansion of greater plasma density in the Southern Hemisphere over the Pacific Ocean. In the Northern Hemisphere, where the northward offset of the dip equator from the geographic equator is less evident, similar though reduced enhancement occurs.

Apart from the role of neutral winds organizing ionospheric structure, in the comprehensive studies by *Jee et al.* [2005], attention is also focused on the importance of plasmaspheric flux, which is one of the least known parameters in the ionospheric modeling, though serves as a distinctive evidence of the coupling between ionosphere and plasmasphere. The pressure difference between ionosphere and plasmasphere drives the refilling of the plasmaspheric flux tubes. However, as they fill up there will be a return flow to the ionosphere mainly at night when the plasma density and temperature in the ionosphere are lower, causing the plasma in the plasmasphere to flow back to the midlatitude ionosphere. The coupling takes place along the magnetic field lines and occurs in the midlatitude region of approximately 20° to 60° in both hemispheres.

Jee et al. [2005] showed that for a downward flux condition, mostly during the night, the plasmaspheric flux can be as important as the neutral wind for maintenance of the nighttime ionosphere. According to simulations based on the SAMI2 model performed by *Chen et al.* [2011], the plasmaspheric downward flux, although not the critical driver, provides plasma source after 2200 LT which maintains the intensity of the WSA density structure. Recently, *Lee et al.* [2013] examined longitudinal trends in the plasmasphere and noted that noticeable annual variations are mostly evident in American sector (30°W–100°W), where the maximum density occurs in December and the minimum in June. Nevertheless, *Lee et al.* [2013] concluded that there is almost no correlation between the annual variations of the ionosphere and the plasmasphere and rather that there is an additional factor to counterbalance the effect of the ionospheric annual variations in the American sector, suggesting that high electron temperature in the topside ionosphere and plasmasphere can be responsible for observed density fluctuations.

5. Summary

Using in situ electron density data registered with the ISL probe on board DEMETER satellite, we have studied spatial and temporal morphology of NPDEs. It is clear that spatial morphology of the introduced I_{NDD} index has a well-defined structure with longitudinal variability strictly correlated with the Earth's magnetic declination. Though proposed approach is very basic, it provides relatively effective way for the localization of NPDEs. I_{NDD} not only allows to clearly distinguish the most common examples of NDPEs, such as WSA and MSNA, but also indicates similar behavior of the equatorial ionosphere, leading to conclusion that all instances are triggered by similar mechanism.

It should be stressed out that in contrast to already published studies focused on WSA and MSNA, presented analysis relates to ionospheric region greatly above the F_2 peak. Even though the measurements are

conducted in the topside ionosphere, coupling between ionosphere and lower layers of the thermosphere is well documented.

With applied method we reckon that higher plasma density in the nighttime hours may be encountered over relatively wide regions what might raise questions about reliability of defined index. The major limitation as well as the weakest point of the proposed approach is the fact that the I_{NDD} is computed at a fixed altitude determined by the satellite orbit, and it does not take into account the effect of the ionospheric layer height change in the diurnal cycle. In the daytime, the neutral wind blows mainly from subsolar point toward poleward direction, while it turns from poleward to equatorward during nighttime. The poleward neutral wind tends to bring the ionospheric layer down to lower altitude, while the equatorward wind raises the layer to higher altitude *Lin et al.* [2010]. As a result, we may encounter an overestimation of the nighttime/daytime N_e difference and I_{NDD} in consequence. Presumably, analyzed difference would be reduced, if we had measurements directly at noon and midnight. Discrepancy between data and model is remarkable; nevertheless, we should take into account that representation of the topside ionosphere derived from IRI is not as accurate as for lower layers. On the other hand, in terms of characteristics of general trend and for the sake of climatological studies, our procedure is acceptable.

Summarizing the discussion it is hard to find one convincing argument, which fully explains observed pattern and behavior of NPDEs. Gathered results show that multiinstrumental analysis are essential for better understanding NPDEs character. It is highly probable that constellation of three satellites, the SWARM mission, launched by ESA in November 2013, can bring new findings to the problem.

Acknowledgments

IRI2012 model used in this work was taken from http://nssdcftp.gsfc.nasa.gov. The authors want to thank all the developers and maintainers for the availability of this tool. The Earth's magnetic field data based on the IGRF model were downloaded from http://www.ngdc.noaa.gov/geomag-web/?model=igrf. The authors would like to thank DEMETER Mission Team and the LPC2E Team for making DEMETER data available. Finally, we would like thank the reviewers for valuable comments, which helped to improve the quality of the paper.

Alan Rodger thanks the reviewers for their assistance in evaluating this paper.

References

Bailey, G. J., M. H. Denton, R. A. Heelis, and S. Venkatraman (2000), A modelling study of the latitudinal variations in the nighttime plasma temperatures of the equatorial topside ionosphere during northern winter at solar maximum, *Ann. Geophys.*, *18*(11), 1435–1446, doi:10.1007/s00585-000-1435-6.

Bilitza, D., L.-A. McKinnell, B. Reinisch, and T. Fuller-Rowell (2011), The International Reference Ionosphere today and in the future, *J. Geod.*, *85*, 909–920, doi:10.1007/s00190-010-0427-x.

Burns, A. G., Z. Zeng, W. Wang, J. Lei, S. C. Solomon, A. D. Richmond, T. L. Killeen, and Y.-H. Kuo (2008), Behavior of the F_2 peak ionosphere over the South Pacific at dusk during quiet summer conditions from COSMIC data, *J. Geophys. Res.*, *113*, A12305, doi:10.1029/2008JA013308.

Burns, A. G., S. C. Solomon, W. Wang, G. Jee, C. H. Lin, C. Rocken, and Y. H. Kuo (2011), The summer evening anomaly and conjugate effects, *J. Geophys. Res.*, *116*, A01311, doi:10.1029/2010JA015648.

Chen, C. H., J. D. Huba, A. Saito, C. H. Lin, and J. Y. Liu (2011), Theoretical study of the ionospheric Weddell Sea Anomaly using SAMI2, *J. Geophys. Res.*, *116*, A04305, doi:10.1029/2010JA015573.

deLarquier, S., J. M. Ruohoniemi, J. B. H. Baker, N. Ravindran Varrier, and M. Lester (2011), First observations of the midlatitude evening anomaly using Super Dual Auroral Radar Network (SuperDARN) radars, *J. Geophys. Res.*, *116*, A10321, doi:10.1029/2011JA016787.

Heelis, R., and W. Hanson (1980), Interhemispheric transport induced by neutral zonal winds in the F region, *J. Geophys. Res.*, *85*(A6), 3045–3047, doi:10.1029/JA085iA06p03045.

Horvath, I. (2006), A total electron content space weather study of the nighttime Weddell Sea Anomaly of 1996/1997 southern summer with TOPEX/Poseidon radar altimetry, *J. Geophys. Res.*, *111*, A12317, doi:10.1029/2006JA011679.

Horvath, I., and E. A. Essex (2003), The Weddell Sea Anomaly observed with the Topex satellite data, *J. Atmos. Sol. Terr. Phys.*, *65*, 693–706, doi:10.1016/S1364-6826(03)00083-X.

Horvath, I., and B. C. Lovell (2009a), Investigating the relationships among the South Atlantic Magnetic Anomaly, southern nighttime midlatitude trough, and nighttime Weddell Sea Anomaly during southern summer, *J. Geophys. Res.*, *114*, A02306, doi:10.1029/2008JA013719.

Horvath, I., and B. C. Lovell (2009b), An investigation of the northern hemisphere midlatitude nighttime plasma density enhancements and their relations to the midlatitude nighttime trough during summer, *J. Geophys. Res.*, *114*, A08308, doi:10.1029/2009JA014094.

Horvath, I., and B. C. Lovell (2010), Investigating the southern daytime midlatitude trough's relation with the daytime Weddell Sea Anomaly during equinoxes, *J. Geophys. Res.*, *115*, A01302, doi:10.1029/2008JA014002.

Hsu, M. L., C. H. Lin, R. R. Hsu, J. Y. Liu, L. J. Paxton, H. T. Su, H. F. Tsai, P. K. Rajesh, and C. H. Chen (2011), The O I 135.6 nm airglow observations of the midlatitude summer nighttime anomaly by TIMED/GUVI, *J. Geophys. Res.*, *116*, A07313, doi:10.1029/2010JA016150.

Jee, G., R. W. Schunk, and L. Scherliess (2005), On the sensitivity of total electron content (TEC) to upper atmospheric/ionospheric parameters, *J. Atmos. Sol. Terr. Phys.*, *67*(11), 1040–1052, doi:10.1016/j.jastp.2005.04.001.

Jee, G., A. G. Burns, Y.-H. Kim, and W. Wang (2009), Seasonal and solar activity variations of the Weddell Sea Anomaly observed in the TOPEX total electron content measurements, *J. Geophys. Res.*, *114*, A04307, doi:10.1029/2008JA013801.

Kakinami, Y., C. H. Lin, J. Y. Liu, M. Kamogawa, S. Watanabe, and M. Parrot (2011), Daytime longitudinal structures of electron density and temperature in the topside ionosphere observed by the Hinotori and DEMETER satellites, *J. Geophys. Res.*, *116*, A05316, doi:10.1029/2010JA015632.

Lebreton, J.-P., et al. (2006), The ISL Langmuir probe experiment processing onboard DEMETER: Scientific objectives, description and first results, *Planet. Space Sci.*, *54*, 472–486, doi:10.1016/j.pss.2005.10.017.

Lee, H.-B., G. Jee, Y. H. Kim, and J. S. Shim (2013), Characteristics of global plasmaspheric TEC in comparison with the ionosphere simultaneously observed by Jason-1 satellite, *J. Geophys. Res. Space Physics*, *118*, 935–946, doi:10.1002/jgra.50130.

Lin, C. H., C. H. Liu, J. Y. Liu, C. H. Chen, A. G. Burns, and W. Wang (2010), Midlatitude summer nighttime anomaly of the ionospheric electron density observed by FORMOSAT-3/COSMIC, *J. Geophys. Res.*, *115*, A03308, doi:10.1029/2009JA014084.

Penndorf, R. (1965), *The Average Ionospheric Conditions Over the Antarctic*, pp. 1–45, AGU, Washington, D. C., doi:10.1029/AR004p0001.

Ren, Z., W. Wan, L. Liu, H. Le, and M. He (2012), Simulated midlatitude summer nighttime anomaly in realistic geomagnetic fields, *J. Geophys. Res.*, *117*, A03323, doi:10.1029/2011JA017010.

Rishbeth, H. (1998), How the thermospheric circulation affects the ionospheric F2-layer? *J. Atmos. Sol. Terr. Phys.*, *60*, 1385–1402.

Rishbeth, H. (2000), The equatorial F-layer progress and puzzles, *Ann. Geophys.*, *18*(7), 730–739, doi:10.1007/s00585-000-0730-6.

Slominska, E., and H. Rothkaehl (2013), Mapping seasonal trends of electron temperature in the topside ionosphere based on DEMETER data, *Adv. Space Res.*, *52*(1), 192–204, doi:10.1016/j.asr.2013.03.004.

Thampi, S. V., C. Lin, H. Liu, and M. Yamamoto (2009), First tomographic observations of the Midlatitude Summer Nighttime Anomaly over Japan, *J. Geophys. Res.*, *114*, A10318, doi:10.1029/2009JA014439.

Thampi, S. V., N. Balan, C. Lin, H. Liu, and M. Yamamoto (2011), Mid-latitude summer nighttime anomaly (MSNA)—Observations and model simulations, *Ann. Geophys.*, *29*(1), 157–165, doi:10.5194/angeo-29-157-2011.

Titheridge, J. E. (1995), Winds in the ionosphere—A review, *J. Atmos. Terr. Phys.*, *57*(14), 1681–1714.

Tsagouri, I., and A. Belehaki (2002), On the nature of nighttime ionisation enhancements observed with the Athens Digisonde, *Ann. Geophys.*, *20*(8), 1225–1238, doi:10.5194/angeo-20-1225-2002.

Venkatraman, S., and R. Heelis (1999), Longitudinal and seasonal variations in nighttime plasma temperatures in the equatorial topside ionosphere during solar maximum, *J. Geophys. Res.*, *104*(A2), 2603–2611, doi:10.1029/1998JA900109.

Zhang, Y., L. J. Paxton, and H. Kil (2013), Nightside midlatitude ionospheric arcs: TIMED/GUVI observations, *J. Geophys. Res. Space Physics*, *118*, 3584–3591, doi:10.1002/jgra.50327.